CENTER FOR
QUANTUM &
TOPOLOGICAL
SYSTEMS

Research symposium

A Tale of Two Valleys

The Hidden Geometry of Excitons

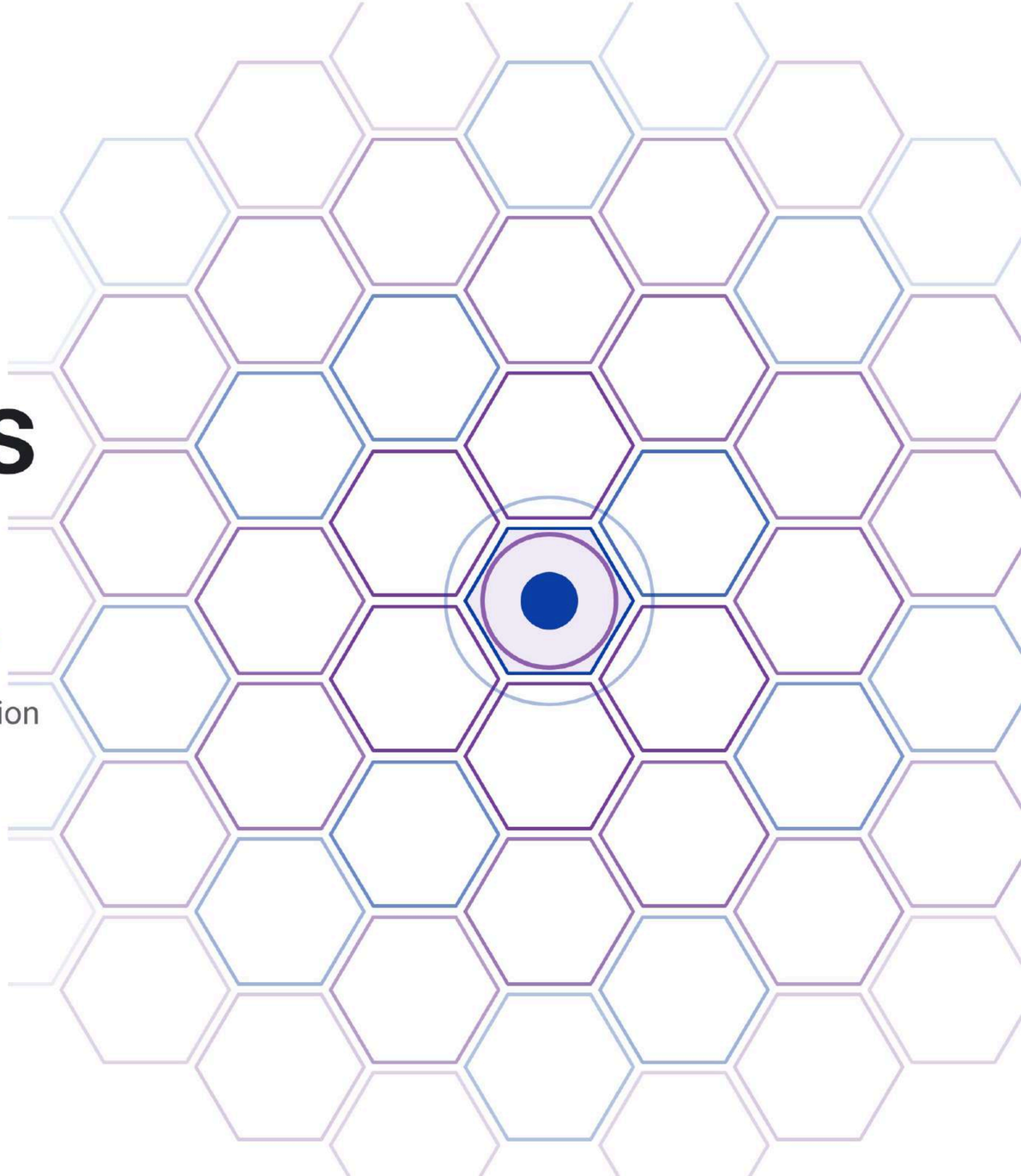
Can we have topological excitons in biased bilayer graphene?

Exciton Berry curvature from a finite-momentum Bethe–Salpeter calculation

Sviatoslav Gladyshev

Supervisor: Dr. Marwa Mannai

Center for Quantum and Topological Systems, NYU Abu Dhabi · Ateno



Motivation

Why excitons?

Bound.

An electron and a hole, held by Coulomb attraction. Approximately a boson at low density.

Neutral.

No net charge current, yet energy and information still move.

Geometric.

Their motion may depend on the geometry of the exciton band.

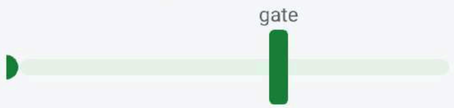
Hypothesis: if the composite has its own band geometry, an electric field could steer how it moves.

Motivation · devices that exist today

Published experiments

Excitons and polaritons already carry information.

Experiment · Bare excitons



Optoexcitonic switch

Gated flow

WSe_2 monolayer · room temperature

Takeaway: excitons can be guided and switched like a signal.

Not: topological, and not graphene.

Jiang et al., ACS Nano 19, 32123 (2025)

Experiment · Polaritons



Polariton transistor

2 × 2 μm²

Polymer in silicon-photonics cavities · room temperature

Takeaway: polaritons switch and amplify light on a chip, in picoseconds.

Not: bare excitons; not topological.

Tassan et al., Light Sci. Appl. 15, 65 (2026)

Experiment · Polaritons



Polariton spin logic

60 μm

Perovskite ($FAPbBr_3$) microcavity · room temperature

Takeaway: polariton spin travels 60 μm and drives a logic gate.

Not: exciton Berry curvature: photonic spin–orbit coupling.

Shi et al., Nat. Mater. 24, 56 (2025)

Experiment · Polaritons



Valley routing

gap ≈ 9 meV

Patterned perovskite valley-Hall lattice · room temperature

Takeaway: K and K' states can be routed in opposite directions.

Not: excitonic topology: the lattice is engineered.

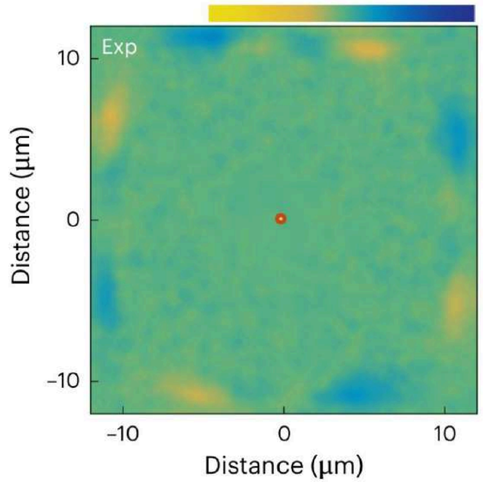
Jin et al., Nat. Commun. 15, 10563 (2024)

All four are working experiments. **None is bilayer graphene, and none uses the Berry curvature of the excitons themselves.**

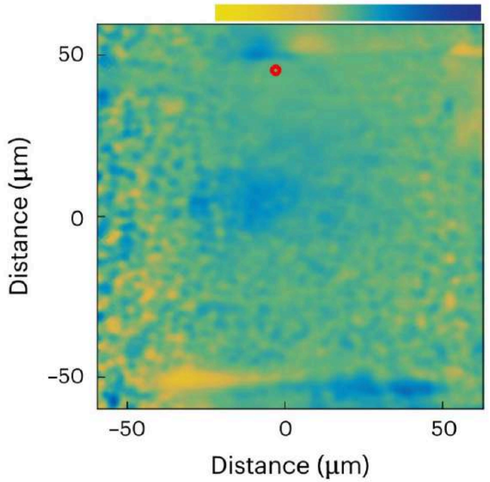
CENTER FOR QUANTUM & TOPOLOGICAL SYSTEMS

Experiment · WS_2

Spin information travels 92 µm at room temperature.



Eight spin domains around the pump (red dot), 20 × 20 µm² cavity



Spin across the cavity, 100 × 100 µm², pump near the top edge

Colour: degree of circular polarization, yellow σ^+ to blue σ^-. Measured, hBN/WS_2/SiN/SiO_2.

92 µm spin-polarized polariton transport at room temperature, with ordinary non-resonant pumping

1. **Bright excitons** in WS_2 mix with guided light into long-lived, fast polaritons.
2. **Dark excitons**, filled by ordinary pumping, act as a built-in source for both TE and TM modes.
3. **Optical spin Hall effect:** TE–TM splitting of the light modes turns linear into circular polarization.

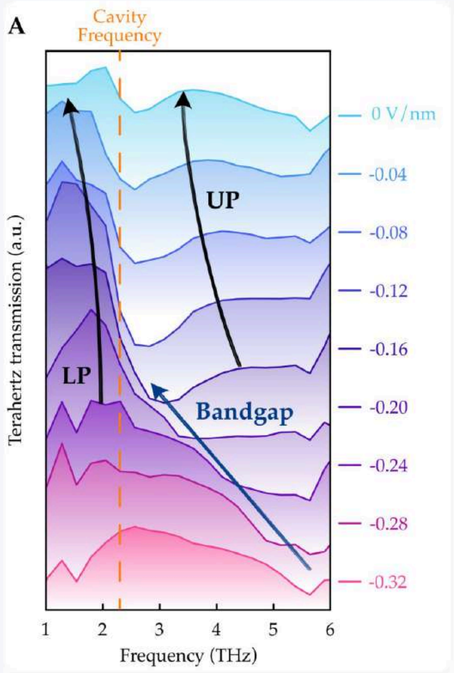
Why it matters: long-range spin transport at room temperature is a step towards spin-polaritonic logic circuits.

Different physics from ours: the spin texture comes from photonic TE–TM splitting in a WS_2 waveguide, not from exciton Berry curvature, and not from bilayer graphene. **It motivates applications; it does not test our mechanism.**

Figure: Research Briefing, Nat. Mater. (2026), © 2026 Shang, Q. et al. · Paper: Q. Shang et al., Nat. Mater. (2026)

Motivation · why biased bilayer graphene?

Bilayer graphene already works inside a cavity.



Experiment · Bilayer graphene

Dual-gated AB bilayer in a terahertz cavity

The gate field D tunes the gap through the cavity frequency. **Ultrastrong coupling, $g/\omega_c \approx 40$ %.**

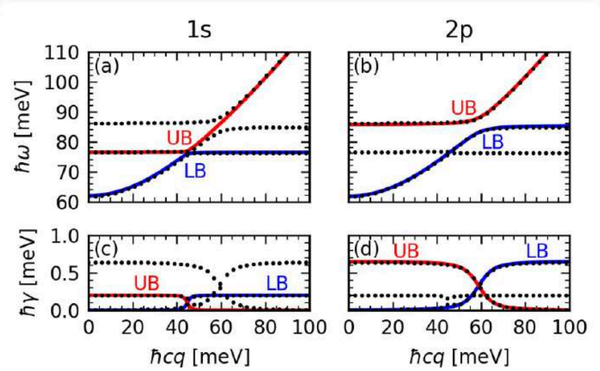
A cavity-induced, **exciton-like state** is pulled out of the electron–hole continuum (LP).

Not: our exciton. Photon-mediated binding at meV gaps and 5 K, not Coulomb excitons.

Helmrich et al., Nature 654, 361 (2026)

Theory · Biased bilayer graphene

Exciton-polaritons tuned by the bias



The bias tunes the polariton branches (UB, LB) and the Rabi splitting. Shown at 100 meV, the bias used in our model.

Not: measured yet, and no exciton geometry.

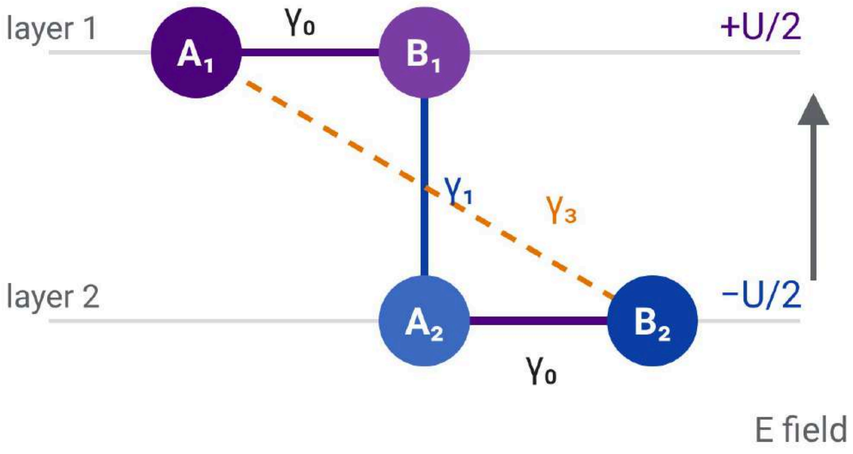
Duarte et al., Phys. Rev. B 111, 075411 (2025)

Experiment: the platform exists. Theory: the bias tunes its polaritons. **Missing: the geometry of the exciton states themselves.**

Figures: Helmrich et al., arXiv:2408.00189 version, n = 0, 5 K (CC BY 4.0) · Duarte et al., arXiv:2502.06640, Fig. 4 (CC BY 4.0)

Established model

Four orbitals and one gate-controlled bias.



$$H(\mathbf{k},U)=\begin{pmatrix} U/2 & -\gamma_0 g & 0 & -\gamma_3 g^* \\ -\gamma_0 g^* & U/2 & \gamma_1 & 0 \\ 0 & \gamma_1 & -U/2 & -\gamma_0 g \\ -\gamma_3 g & 0 & -\gamma_0 g^* & -U/2 \end{pmatrix}$$

$$g(\mathbf{k})=\sum_{j=1}^{3} e^{i\mathbf{k}\cdot\boldsymbol{\delta}_j}, \qquad g(\mathbf{K}+\mathbf{p}) \simeq -\tfrac{\sqrt{3}\,a}{2}\,(p_x - i p_y)$$

A_1, B_1 · A_2, B_2	carbon p_z orbitals of the top and bottom layers
γ_0 = 3.0 eV	in-plane nearest-neighbour hopping
γ_1 = 0.40 eV	vertical B_1–A_2 (dimer) coupling
γ_3 = 0.30 eV	skew A_1–B_2 hopping: trigonal warping
±U/2	layer potentials from the gate: the only place the bias U enters

Published gap · model bands

A band gap you can dial.

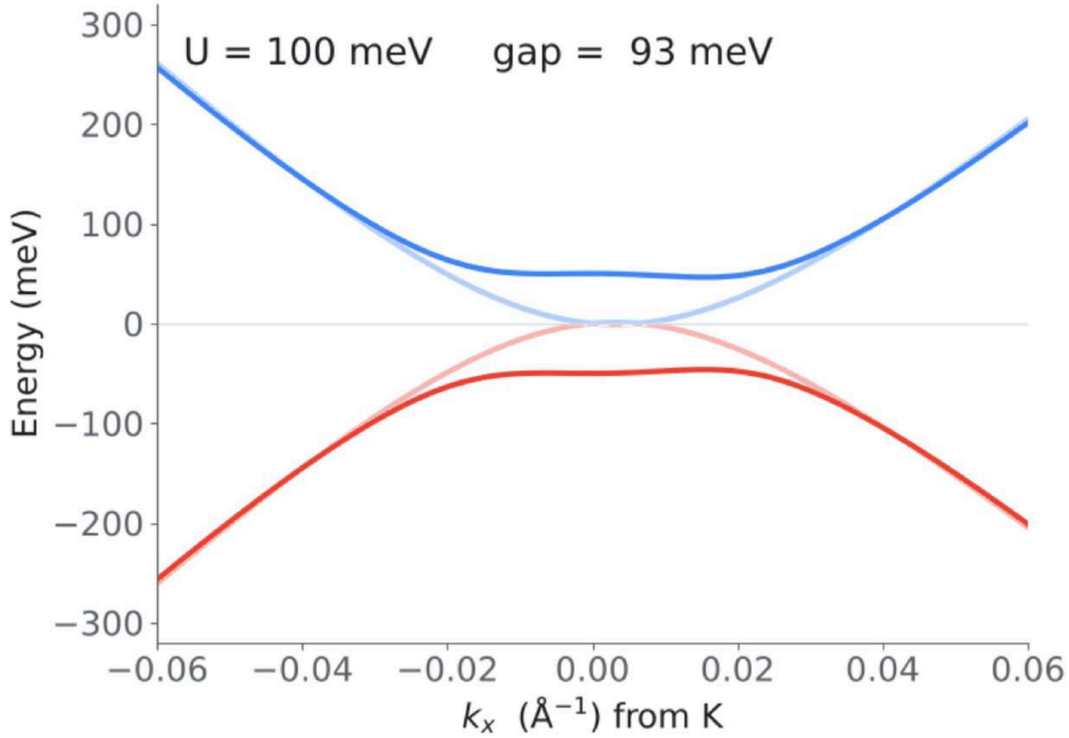
At U = 0: two bands touch at K and K', with approximately parabolic dispersion.

$$E_{\pm}(\mathbf{p}) \simeq \pm\sqrt{\frac{U^2}{4} + \left(\frac{\hbar^2 p^2}{2m^*}\right)^2} \quad (\gamma_3 = 0,\ U \ll \gamma_1)$$

With bias U: a gap of order U opens, up to ≈ 300 meV (DFT). We use **U = 100 meV**.

Mexican hat: the band edge moves off K onto a small ring around it.

> **Why it matters:** excitons are built from these conduction and valence states, so both their energies and their Bloch eigenstates enter the calculation.



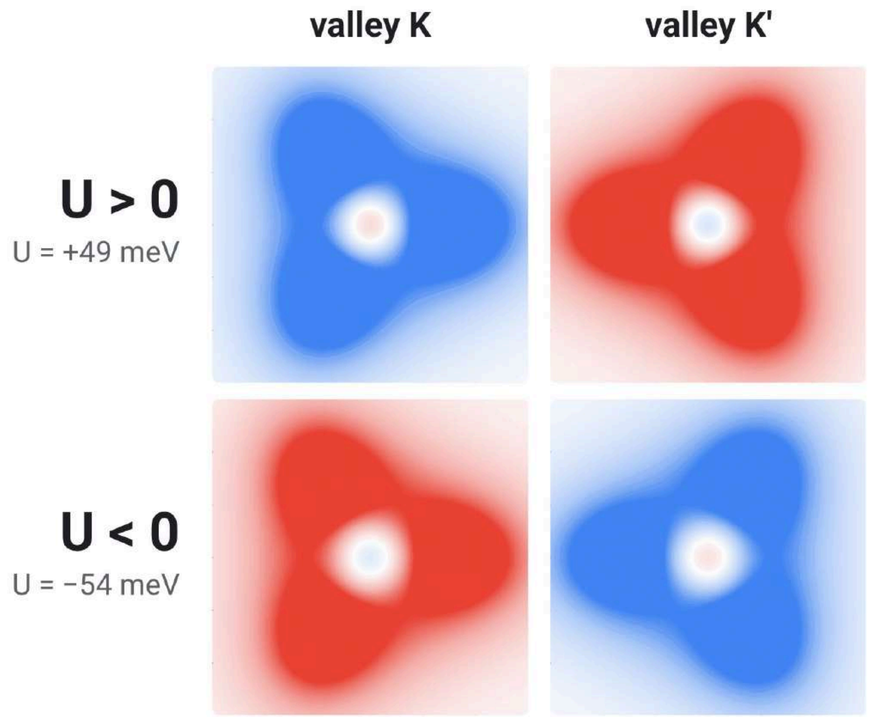
Bold: U = 100 meV, the value used · **faded: U = 0**, bands touch

Gap: Sauer & Pedersen (DFT) · Plot: author's four-band model, γ_0 = 3.0, γ_1 = 0.40, γ_3 = 0.30 eV

Established physics · derived here

Electronic Berry curvature flips with the bias.

Electronic Berry curvature Ω(k) acts like a magnetic field in momentum space for one Bloch band. Integrated over one valley, it gives the valley Chern number.



Conduction band, k_x, k_y from −0.03 to 0.03 $Å^{-1}$ around each valley.

Reversing U swaps the colours; K and K' are always opposite.

$$C_{\pm}^{(K)} = \mp \operatorname{sgn} U, \qquad C_{\pm}^{(K')} = -\,C_{\pm}^{(K)}$$

conduction	K	K'
U > 0	−1	+1
U < 0	+1	−1

Opposite in K and K', so the total Chern number is zero; reversing U reverses both.

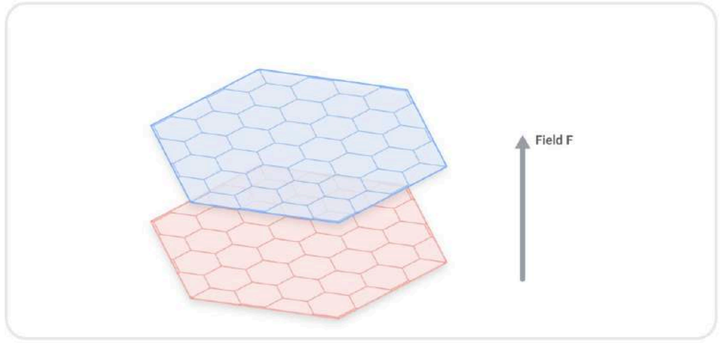
> This is **electronic** Berry curvature, in k. **Exciton** Berry curvature, in Q, is a separate calculation.

Author's two-band model · U from +100 to −100 meV · blue: negative, red: positive · Appendix A: Chern derivation

CENTER FOR QUANTUM & TOPOLOGICAL SYSTEMS

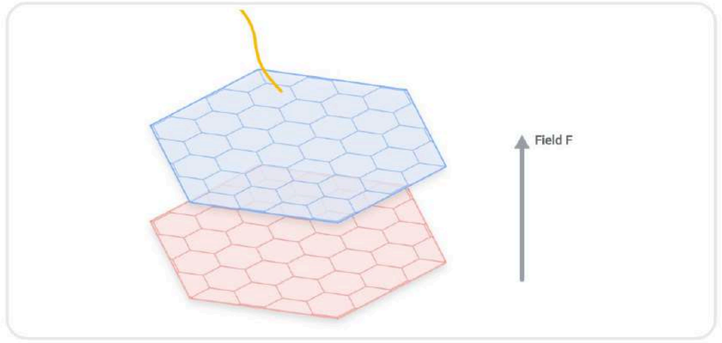
Schematic

The story, in one picture.



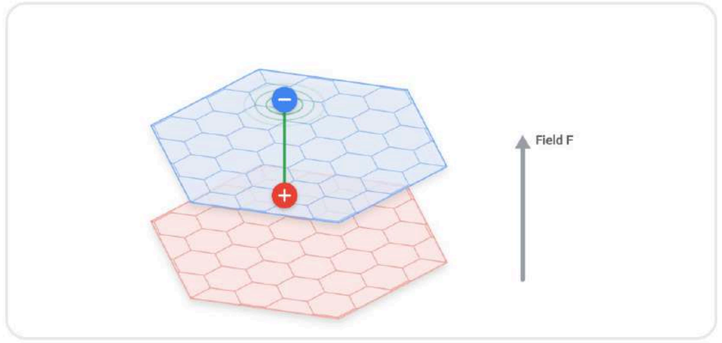
1 · Bilayer **Two graphene sheets, AB-stacked**

A perpendicular field opens a tunable gap.



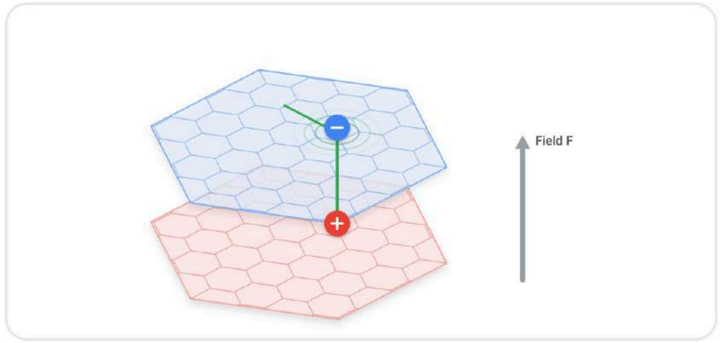
2 · Light in **A photon arrives**

Its energy creates an electron–hole pair.



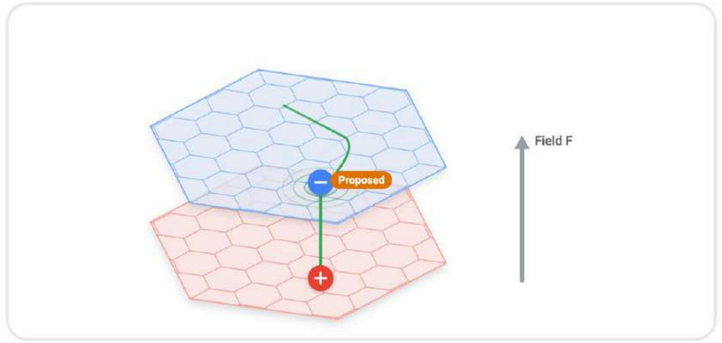
3 · Bind **The pair binds into an exciton**

Drawn with the electron on top. Real states mix layers.



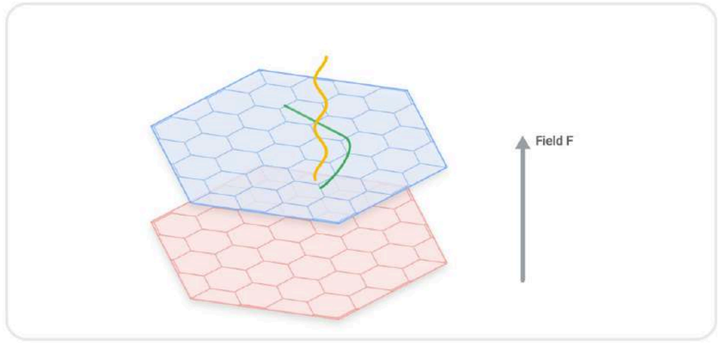
4 · Move **It travels as one neutral particle**

No net charge, but it carries energy.



5 · Bend? **Does its path bend sideways?**

Our open question: exciton Berry curvature.



6 · Light out **It recombines and glows**

A photon leaves, almost straight up.

Established physics

A composite boson with its own momentum Q.

Bare exciton

Electron plus hole, bound by Coulomb attraction.

Approximately bosonic at low density, when pairs do not overlap. This talk is about these.

Exciton-polariton

Exciton strongly coupled to a confined photon.

Part light, part matter. It needs a cavity or similar structure, so its physics differs from a bare exciton.

Centre-of-mass momentum. Every pair in one exciton state shares the same total momentum.

$$\text{electron at } \mathbf{k} + \mathbf{Q}/2, \quad \text{valence state } \mathbf{k} - \mathbf{Q}/2, \quad \text{pair momentum } \mathbf{Q}$$

Being bosonic does **not** imply condensation, topological order or fault-tolerant transport.

Established method

Solving for excitons at finite momentum Q.

$$|X_S(\mathbf{Q})\rangle = \sum_{\mathbf{k},c,v} A^S_{\mathbf{k}cv}(\mathbf{Q})\; c^\dagger_{c,\mathbf{k}+\mathbf{Q}/2}\; c_{v,\mathbf{k}-\mathbf{Q}/2}\; |\mathrm{GS}\rangle$$

A superposition of electron–hole pairs, all with total momentum Q.

$$\sum_j \Big[\big(E_{c_i,\mathbf{k}_i+\frac{\mathbf{Q}}{2}} - E_{v_i,\mathbf{k}_i-\frac{\mathbf{Q}}{2}}\big)\delta_{ij} - K^d_{ij}(\mathbf{Q}) + 2K^x_{ij}(\mathbf{Q})\Big] A^S_j = E_S(\mathbf{Q})\, A^S_i$$

$$i \equiv (\mathbf{k}, c, v): \quad 2 \text{ valence} \times 2 \text{ conduction} = 4 \text{ transitions per } \mathbf{k}$$

1 Independent electron–hole excitation energies

2 Screened Coulomb attraction K^d: binds the pair

3 Electron–hole exchange K^x: repulsive, couples K and K'

Output: exciton energies $E_S(Q)$ and wavefunctions $A^S(Q)$. Exciton Berry curvature needs these weights *and* the Bloch states they multiply.

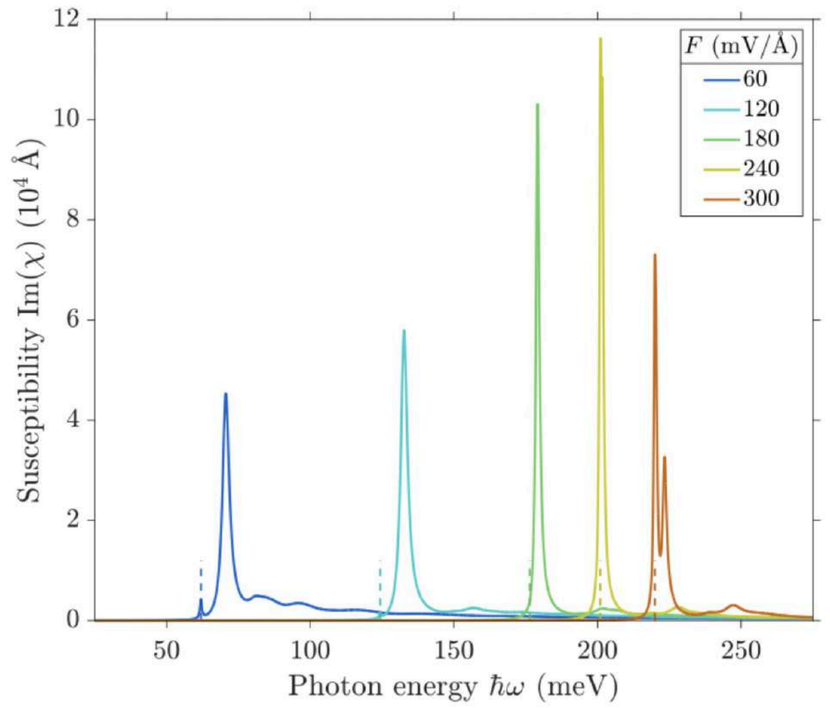
Why finite Q? Exciton Berry curvature describes how the exciton states change with Q, so the BSE is solved on a grid of Q around Q = 0.

Appendix B: exciton mathematics · Appendix C: kernels and screening used here

Excitons · published optics

Published

Bright, dark, and a field-driven crossing.



240 mV/Å

Dark and bright excitons swap order, in suspended and hBN-encapsulated samples alike. The crossing changes which state couples to light; on its own it is not a topological transition.

This work · model, U = 100 meV

Our lowest doublet is optically weak: ≈ 0.14 of the dipole strength of the brightest of the six lowest states (456-point check grid). No field sweep, so no crossing is claimed.

Dark states matter in devices too: out-of-plane dark excitons drive the WS_2 spin currents. Different material, different mechanism.

Figure: Sauer & Pedersen, Phys. Rev. B 105, 115416 (2022)

Main results

Electronic valley Chern numbers are established.

Can we have topological excitons in biased bilayer graphene?

I calculated the Berry curvature of the exciton states themselves, as a function of the exciton momentum Q.

This work · model calculation

From the Hamiltonian to exciton Berry curvature.

Numerical calculations implemented in Python

1 Tight-binding Hamiltonian
Four-orbital H(k, U) over the whole Brillouin zone

→

2 Diagonalize
Electronic energies and Bloch eigenstates

→

3 Finite-Q BSE Hamiltonian
Screened direct attraction + exchange

→

4 Solve
Exciton energies $E_S(Q)$ and wavefunctions

→

5 Lowest doublet
Two nearly degenerate excitons, isolated from the rest

→

6 Exciton Berry curvature
Non-Abelian, from gauge-covariant Wilson loops

≈ 8,000 coupled electron–hole configurations in the largest calculation, with both valleys in one Bethe–Salpeter matrix.

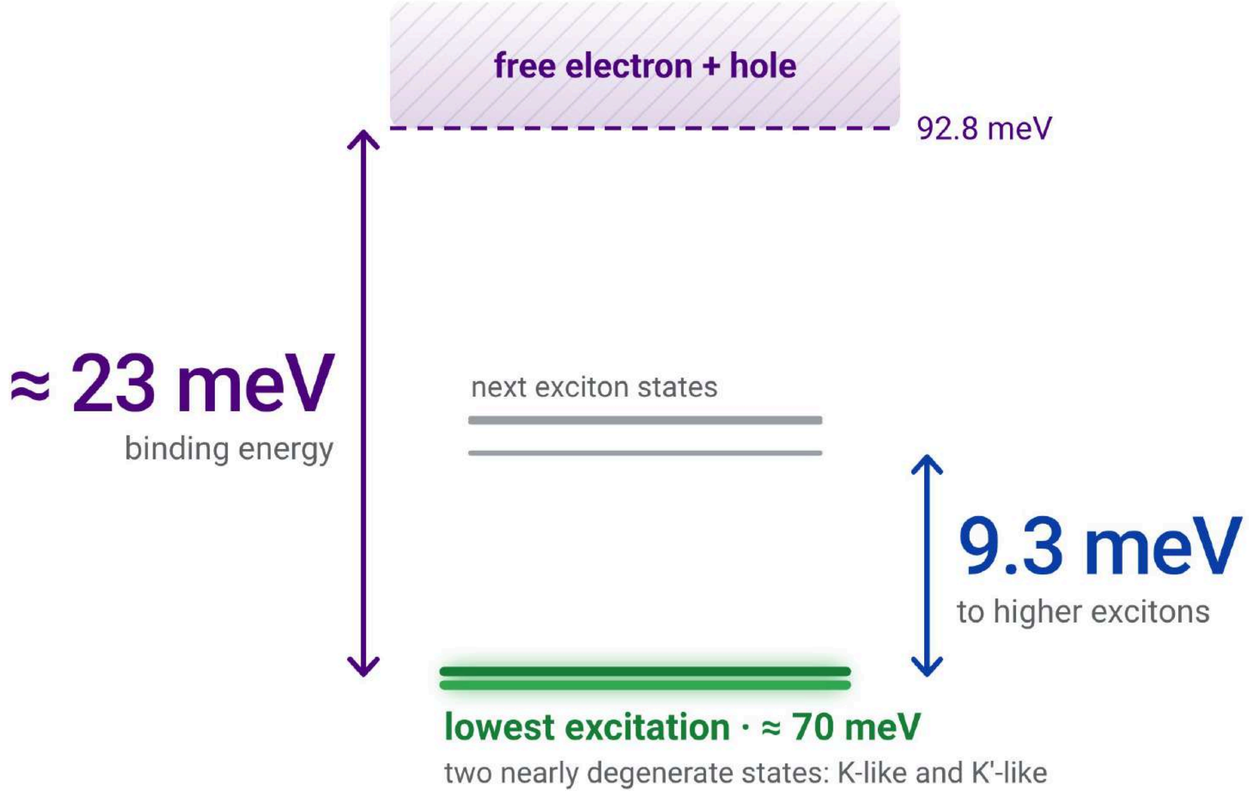
Model parameters (assumed, not a specific device)

γ_0 = 3.0 eV · γ_1 = 0.40 eV · γ_3 = 0.30 eV · a = 2.46 Å
U = 100 meV · κ = 4.5 · layer spacing 3.35 Å

Electron at k + Q/2, valence state at k − Q/2 · Appendix C: kernels, screening and conventions

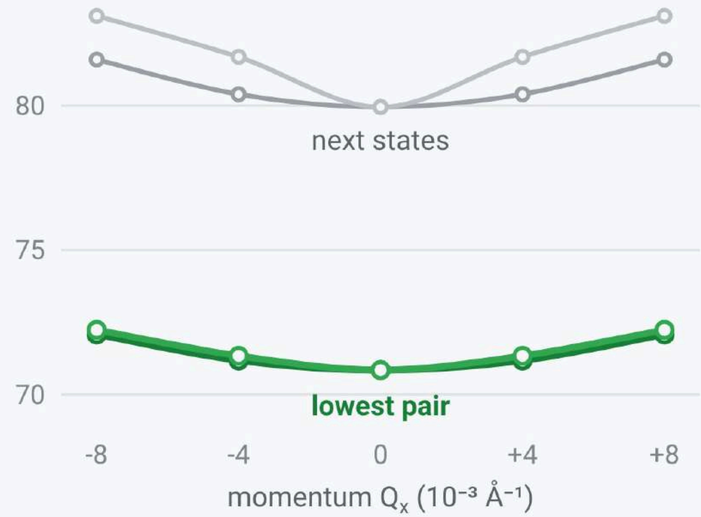
This work · model calculation

The lowest excitons form a bound, nearly degenerate pair.



When the exciton moves

its energy rises like a particle with mass, and the pair splits slightly.



864 k points, so 70.8 meV at Q = 0

Model results, not measurements · ladder: 1980 BSE k points, screening on 5712 k

CENTER FOR QUANTUM & TOPOLOGICAL SYSTEMS

This work · model calculation

Opposite Exciton Berry Curvature in the Two Valleys

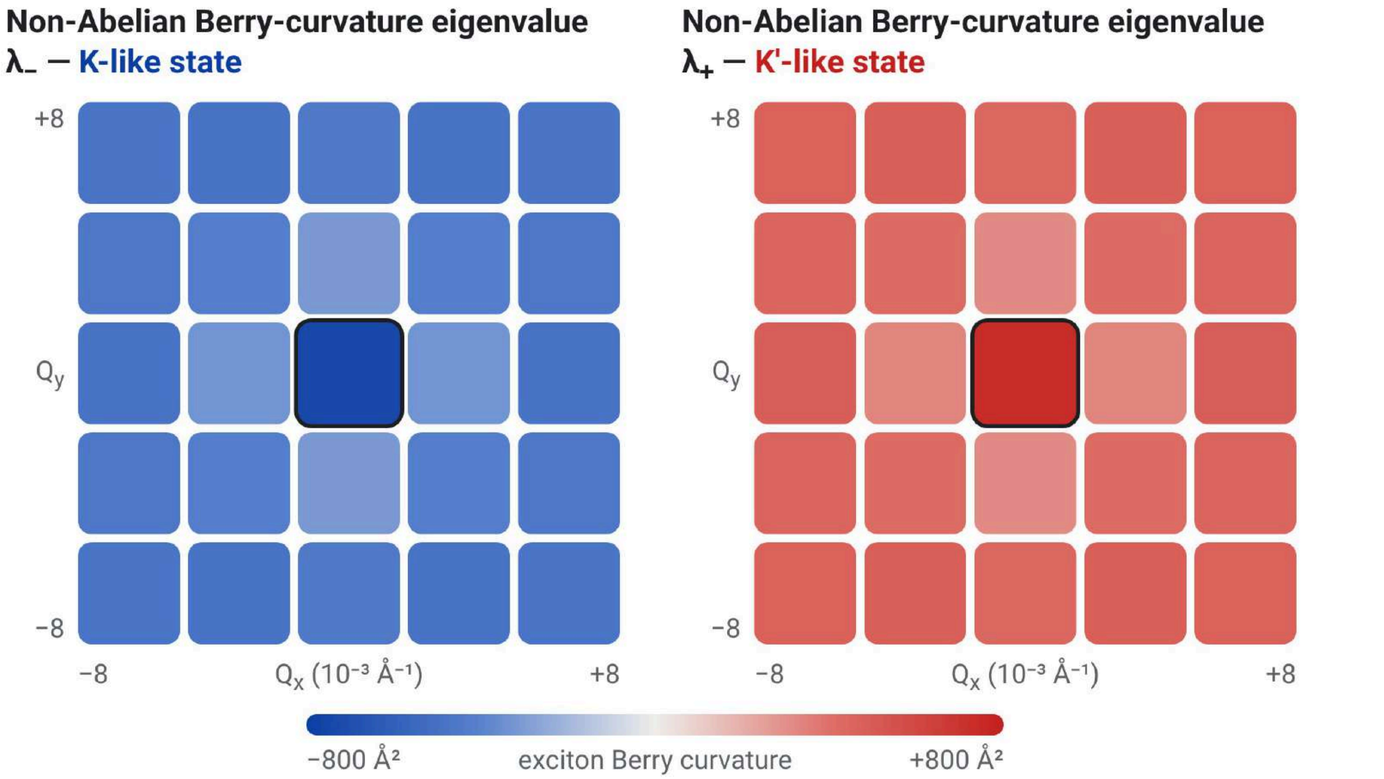
Exciton Berry curvature near Q = 0

≈ ±730 Å²

Blue (−) and red (+): opposite signs for the K-like and K'-like states, each > 99.9 % in one valley.

Stronger colour = larger magnitude. Largest at Q = 0 (outlined).

> **The two lowest excitons are nearly degenerate, so their Berry curvature is calculated together.** $\lambda_{\pm}$ are eigenvalues of their 2 × 2 Berry-curvature matrix, not Berry curvatures of two separate bands.
>
> Calculated near Q = 0, not across the full exciton Brillouin zone.



Each tile is one calculated Q point (a small Wilson loop, 864 k points); colour set by its value. No interpolation.

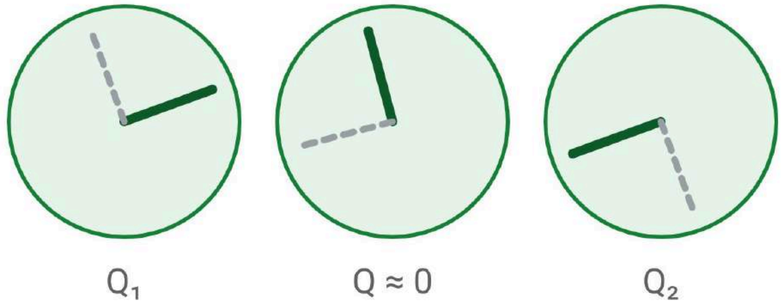
This work · model calculation

Because the two lowest excitons are nearly degenerate, we calculate the Berry curvature of their combined subspace.

$$M_{ST}(\mathbf{Q},\mathbf{Q}') = \sum_{\mathbf{k}} \sum_{cv,c'v'} A^{S*}_{\mathbf{k}cv}(\mathbf{Q})\, A^{T}_{\mathbf{k}c'v'}(\mathbf{Q}') \underbrace{\langle u_{c,\mathbf{k}+\mathbf{Q}/2} | u_{c',\mathbf{k}+\mathbf{Q}'/2}\rangle}_{\text{electron}} \underbrace{\langle u_{v',\mathbf{k}-\mathbf{Q}'/2} | u_{v,\mathbf{k}-\mathbf{Q}/2}\rangle}_{\text{hole}}$$

Exciton overlap between neighbouring Q: BSE weights × electron and hole Bloch-state overlaps, so arbitrary phases cancel.

same smooth plane: span{X_1, X_2}



One energy state: jumps between nearby Q.

Two-state subspace: smooth everywhere.

$$M = L\,\Sigma\,R^{\dagger} \;\Rightarrow\; \mathcal{U} = LR^{\dagger}, \qquad \mathcal{W} = \mathcal{U}_{12}\,\mathcal{U}_{23}\,\mathcal{U}_{34}\,\mathcal{U}_{41}$$

$$\lambda_{\pm}(\mathcal{F}_{xy}) \simeq -\frac{\arg\ \mathrm{eig}_{\pm}(\mathcal{W})}{\delta Q_x\, \delta Q_y}$$

The Wilson loop *W* gives the 2 × 2 Berry-curvature matrix *F*. A U(2) basis change inside the doublet only rotates *W* and *F*: $\lambda_{\pm}$ are basis-independent.

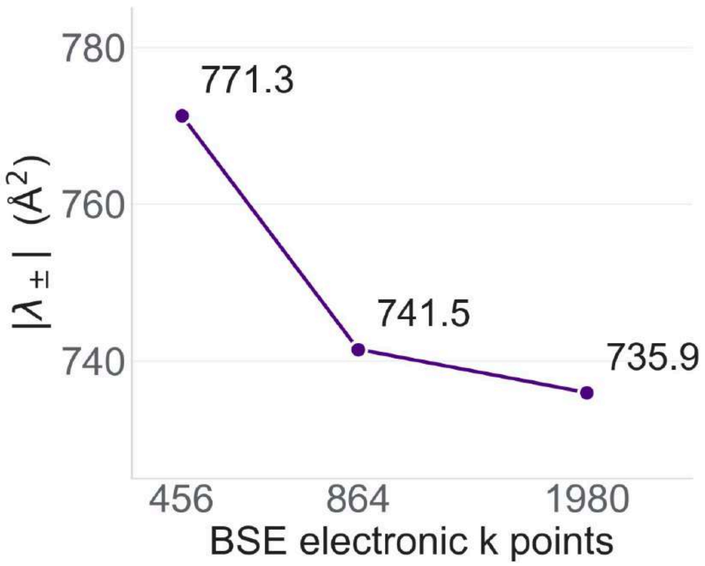
Two-state subspace	Berry-curvature eigenvalues $\lambda_{\pm} \approx \pm 730$ Å²
Single energy branches	Berry curvature compatible with zero

Appendix C: overlap diagnostics · Schematic on the left; values from lattice_local_map.npz

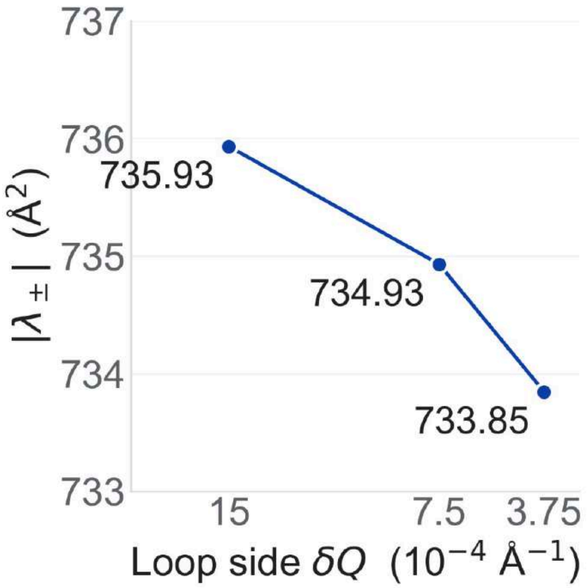
This work · model calculation

Stable under grid refinement and gauge changes.

(a) Electronic k grid, loop side 1.5 × 10⁻³ Å⁻¹



(b) Loop size, 1980 k points, RPA 7



A finite Wilson loop measures the average Berry-curvature flux through it; smaller loops approach the local value at Q = 0. The scale, ≈ 730–770 Å², is stable.

- **Gauge invariant:** random phases of the Bloch states leave the Berry curvature unchanged
- **Basis independent:** random U(2) rotations of the doublet leave $\lambda_{\pm}$ unchanged
- **Screening and exchange:** finer screening grid and more reciprocal vectors change |λ| by < 0.01 Å²
- **Isolated doublet:** ≥ 9 meV below the next exciton everywhere on the map
- **Solver:** iterative results agree with dense diagonalization

Remaining approximations: static screening, no GW, Tamm–Dancoff, model orbitals. Not yet converged to the last digit.

Appendix C: full convergence tables · all validation checks

This work · model calculation

What we calculated, and what remains open.

What we calculated

1. Opposite Berry-curvature eigenvalues for the lowest exciton doublet, $\lambda_{\pm} \approx \pm 730$ Å² near Q = 0. Reversing U swaps the valleys (one coarse-grid check).

2. Strong valley polarization: each eigenvalue belongs to a state that is > 99.9 % K or K'.

3. A nearly degenerate lowest doublet, ≈ 9 meV below the next exciton states.

What remains open

4. Global exciton topology. The calculation covers $|Q_x|, |Q_y| \leq 0.008$ Å^{-1}. No Chern number or other global invariant has been calculated.

5. A measurable transport response, such as valley-selective sideways drift: not yet calculated or measured.

6. Device-level modelling: gates, substrate, disorder and a realistic dielectric environment.

In this model of biased bilayer graphene, the lowest exciton doublet has substantial, valley-contrasting non-Abelian Berry curvature. Whether this leads to a global excitonic topological phase or a measurable transport effect remains an open question.

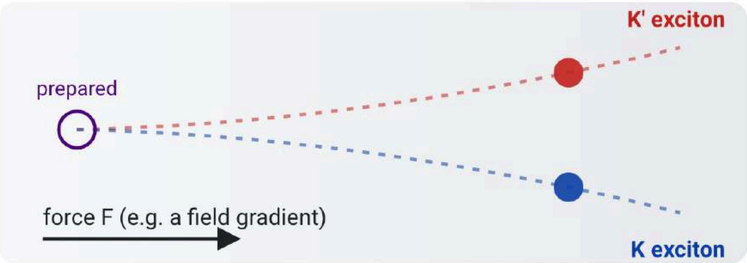
Not in the model: GW corrections · dynamic screening · spin–orbit coupling · triplets · phonons and disorder · full ab initio dielectric response · calibrated device environment

Towards applications · research directions, not results

Proposal · next steps

Can exciton geometry steer information?

A Valley-dependent exciton transport



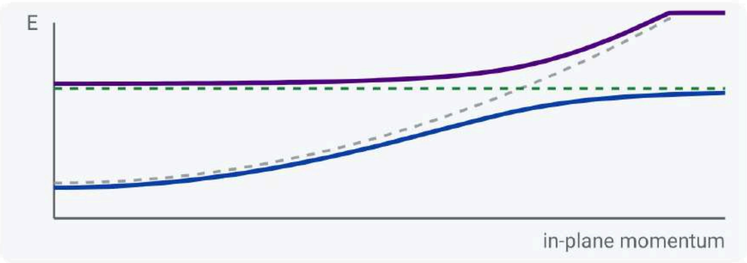
Cartoon of the semiclassical expectation. Not calculated.

Under a suitable force, Berry curvature adds a velocity perpendicular to the force: opposite in K and K'. For our doublet this needs non-Abelian dynamics.

Would need:

- non-Abelian wavepacket dynamics
- a realistic force on a neutral exciton
- intervalley mixing and relaxation

B Electrically tunable BLG exciton-polaritons



upper and **lower polariton**, photon, exciton (moves with bias). Schematic only.

Coupled to cavity photons, these excitons could form polaritons tuned by the gate. Our lowest doublet is optically weak; brighter states may dominate.

Would need:

- optical dipole matrix elements
- light–matter coupling g
- cavity detuning
- Hopfield mixing
- linewidths and losses

Already demonstrated elsewhere: spin carried 60–92 µm (perovskite, WS_2) · valley routing (perovskite lattice) · BLG ultrastrongly coupled to a cavity (THz) · theory: exciton quantum geometry can enhance diffusion (Thompson et al., Nat. Commun. 16, 11448 (2025)). Details: backup.

CENTER FOR QUANTUM & TOPOLOGICAL SYSTEMS

BEYOND THE LAB

Ateno AX

Robots need a map where GPS fails.

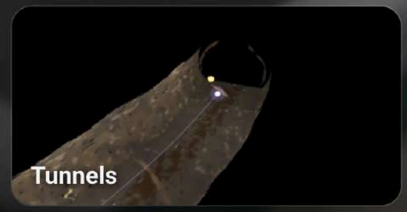
A dedicated chip for on-device 3D mapping: robots and drones build and render Gaussian-splat maps as they move, with no datacenter GPU.

173,161
Gaussians in one 1080p frame on our FPGA prototype

3.9×
faster per frame in 10 days: 1.02 s → 262 ms

Next
silicon tape-out with design partners; no chip yet


A Gaussian-splat scene


Tunnels


Warehouses

CENTER FOR QUANTUM & TOPOLOGICAL SYSTEMS

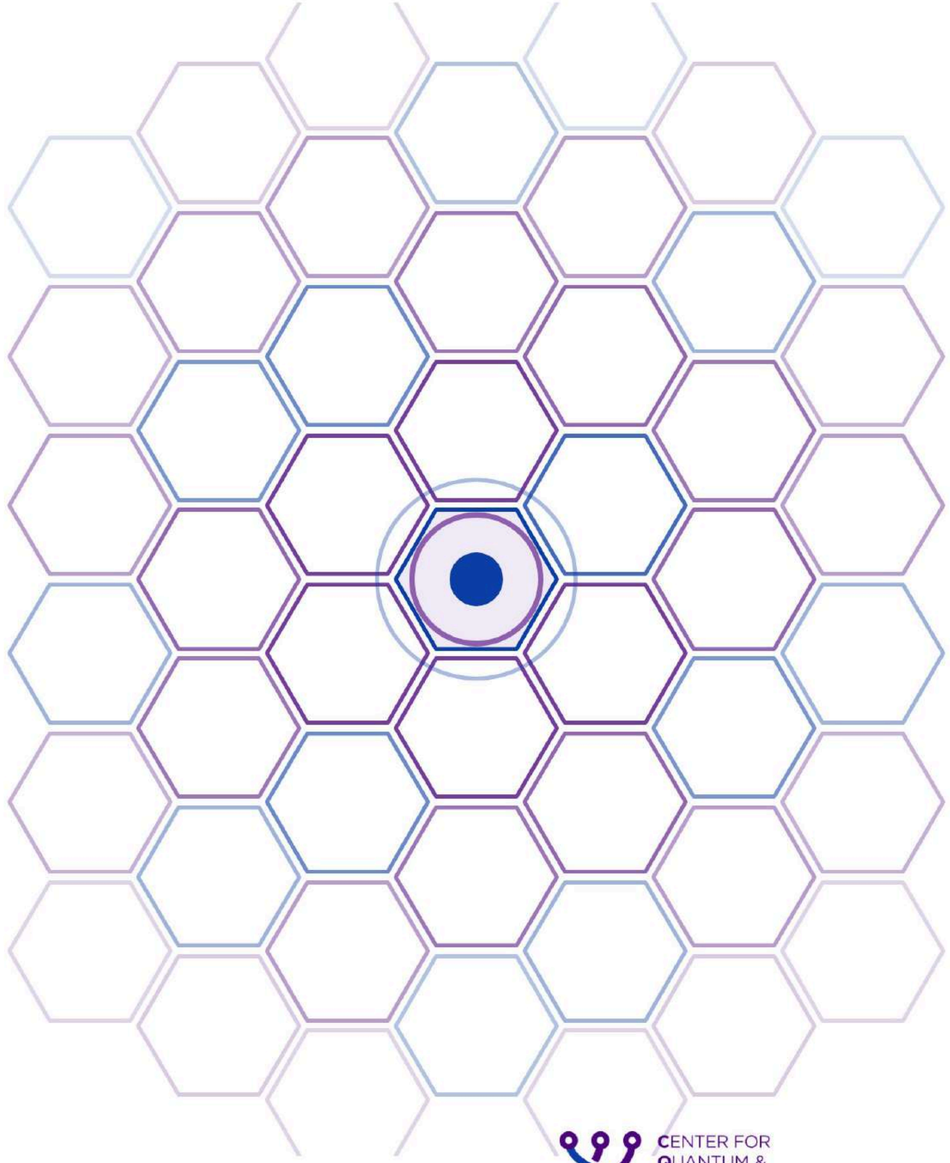
Conclusion

Can we have topological excitons in biased bilayer graphene?

- **Established physics:** electronic valley Chern numbers that reverse with the bias; bright and dark BLG excitons; room-temperature polariton spin transport; BLG in a THz cavity
- **Our calculated results:** opposite exciton Berry curvature, $\lambda_{\pm} \approx \pm 730$ Å² near Q = 0, for a nearly degenerate, valley-polarized lowest doublet
- **Remaining questions:** a global exciton invariant, a measurable transport response, and device-level modelling

Thank you.

With thanks to my supervisor, Dr. Marwa Mannai, and CQTS, NYU Abu Dhabi



CENTER FOR QUANTUM & TOPOLOGICAL SYSTEMS

References

Sources.

Foundations and methods

M. O. Sauer & T. G. Pedersen, Phys. Rev. B 105, 115416 (2022).

C.-H. Park & S. G. Louie, Nano Lett. 10, 426 (2010).

E. McCann & M. Koshino, Rep. Prog. Phys. 76, 056503 (2013).

E. McCann & V. I. Fal'ko, Phys. Rev. Lett. 96, 086805 (2006).

R. Yu, X.-L. Qi, A. Bernevig, Z. Fang & X. Dai, Phys. Rev. B 84, 075119 (2011). Wilson loops.

T. Fukui, Y. Hatsugai & H. Suzuki, J. Phys. Soc. Jpn. 74, 1674 (2005).

Exciton Berryology, arXiv:2507.22983 (2025).

Experiments

Q. Shang et al., Nat. Mater. (2026), doi:10.1038/s41563-026-02782-5.

J. Zúñiga-Pérez & G. Malpuech, Nat. Mater. research briefing (2026).

F. Helmrich et al., Nature 654, 361 (2026).

Y. Shi et al., Nat. Mater. 24, 56 (2025).

F. Jin et al., Nat. Commun. 15, 10563 (2024).

P. Tassan et al., Light Sci. Appl. 15, 65 (2026).

Z. Jiang et al., ACS Nano 19, 32123 (2025).

Theory and context

V. G. M. Duarte et al., Phys. Rev. B 111, 075411 (2025).

J. J. P. Thompson et al., Nat. Commun. 16, 11448 (2025).

H. Davenport, F. Schindler & J. Knolle, Phys. Rev. B 113, 115102 (2026).

T. Eini et al., Phys. Rev. Lett. 134, 196903 (2025).

PolArt project, EIC Pathfinder, grant 101130304.

Figures from other work: Sauer & Pedersen (PRB 105, 115416), Helmrich et al. (CC BY 4.0), Duarte et al. (CC BY 4.0), Shang et al. via the Nat. Mater. research briefing (© 2026 the authors).

CENTER FOR QUANTUM & TOPOLOGICAL SYSTEMS